Adsorption of Hg^{2+}
onto Novel Mesocellular Foams Silica Functionalized
with Disodium Ethylenediaminetetraacetate:
Thermodynamics, Isotherm, and Kinetics Studies

Xiao-Dong, Li

Department of Basic Science, Jilin Jianzhu University, 5088 Xincheng Street, Changchun 130118,
Jilin Province, P.R. CHINA

Qing-Zhou, Zhai*+

Research Center for Nanotechnology, Changchun University of Science and Technology, Changchun 130022,
7186 Weixing Road, Jilin Province, P.R. CHINA

ABSTRACT: *Mercury is one of the most important heavy metal elements of environmental pollution, and it is very important for its control. MesocCllular Foam (MCF) silica was prepared by hydrothermal method, and the prepared material was characterized by Powder X-Ray Diffraction (XRD), Scanning Electron Microscopy (SEM), 77 K low-temperature nitrogen gas adsorption-desorption. Herein, the authors aimed to improve the adsorptive performance of MCF against mercury ions through a functionalization using disodium ethylenediaminetetraacetate (EDTA-Na₂). Our novel material was then used in the batch adsorption of Hg^{2+}, where the maximum conditions were reached after 35 minutes of contact time at pH 3 with the adsorbent weight of 0.1 g. The maximum adsorption amount of Hg^{2+} in the aqueous phase was 139.64 mg Hg^{2+} / g (modified MCF). The maximum desorption ratio of Hg^{2+} was 75.23% achieved by using 0.1 mol/L hydrochloric acid solution. The process for the adsorption of Hg^{2+} conforms to the quasi-second-order adsorption kinetics and Langmuir adsorption isotherm. The results of the low-temperature N_2 adsorption-desorption curve at 77 K showed that Hg^{2+} had entered the MCF pore channels. This novel material is effective in removing Hg^{2+} from the water medium via batch adsorption.*

KEYWORDS: *Hg^{2+}; MCF; Disodium ethylenediaminetetraacetate; Adsorption; Modification; Quasi-second-order kinetics; Adsorption kinetics; Langmuir adsorption isotherm.*

INTRODUCTION

Rapid development of industries (i.e. metallurgy, mining, chemicals, and electrical instruments) could potentially increase the discharge of heavy metal waste to the environment, resulting in heavy metal pollution in water [1-3]. Of these, mercury ion pollution is the most deleterious problem to the environment and the human body [4].

Following the conversion of mercury substances or its ions by microorganisms, organic mercury might pose a threat to human health by damaging the nervous system and causing systemic damage. Not only to humans, but mercury is also found harmful to plants and aquatic organisms [3,4].

In response to the stated problem above, several methods have been proposed to remove the heavy metal ions from water medium, such as ion exchange, biological restoration, and chemical precipitation [5-10], but these methods are either impractical or cause secondary pollution to the environment. On the contrary, heavy metal adsorption has been claimed as a simple technique that does not produce secondary pollution [11-22]. The previously cited works have reported various adsorbent materials, yet practical limitations are still found. For example, activated carbon which is effective for heavy metal adsorption [22], is difficult to be regenerated and expensive. Moreover, it can only be used to treat lower concentrations of sewage and less sewage [10, 11]. Other examples include rice husk and coal fly ash which have drawbacks in terms of their adsorptive performance [2, 10]. Thus, it is still important to investigate new adsorbents.

At the end of the 20th century, the synthesis of nano-mesoporous materials as a new generation of adsorbent materials attracted great interest. Mesocellular foams (MCF), a novel mesoporous silica material, could be synthesized by molecular self-assembly allowing to control its pore size [23-25]. Compared to the traditional zeolite molecular sieve, this kind of mesoporous material has better characteristics in regard to its pore structure, specific surface area, high surface energy, and higher pollutant uptake [26-27].

In this work, MCF was prepared by hydrothermal method along with its functionalization using ethylenediaminetetraacetate (EDTA). Several reports have employed EDTA for functionalizing the adsorbent material which is successful in improving the heavy metal uptake [22]. The adsorbent prepared in this paper is a novel material that has been established to adsorb Hg^{2+} from wastewater. The adsorption kinetics, isotherms, and thermodynamics of the Hg^{2+} uptake process were also investigated.

EXPERIMENTAL SECTION
Materials
Poly (ethylene glycol)-block-poly(propylene glycol)-block-poly (ethylene glycol) (EG_{20}-PG_{40}-EG_{20}) with P123 template and average molecular weight of 5800 (Aldrich, USA) was used for the MCF synthesis. Ethylenediamine tetraacetic acid-disodium ($EDTA$-Na_2), hydrochloric acid, 1,3,5-trimethylbenzene (TMB), anhydrous ethanol, nitric acid, NH_4Cl, and ammonia water were procured from Beijing Chemical Plant, China. Other chemicals included tetraethyl orthosilicate (TEOS) (Shanghai Chemical Reagent Company, China Pharmaceutical Group), mercury nitrate hydrate ($Hg(NO_3)_2 \cdot 1/2 \ H_2O$) (Taixing Chemical Reagent Factory, China), 2-[(5-bromo-2-pyridyl) azo]-5-diethylaminophenol (5-Br-PADAP) (Tianjin Guangfu Fine Chemical Research Institute, China), and Sodium dodecyl sulfate ($C_{12}H_{25}SO_4Na$) (Chinese Pharmaceutical Group Chemical Reagent Co., Ltd., China).

Synthesis of MCF by hydrothermal method
The hydrothermal method used for the synthesis of MCF was based on the previous literature with several modifications [28]. P123 (2 g) was dissolved in 15 g H_2O and 60 g hydrochloric acid solution 2 mol/L. The solution was stirred at constant heat (40°C) until completely dissolved, followed by a slow addition of 4.25 g TEOS. After homogenization, 1.5 g of 3,5-trimethylbenzene (TMB, quality ratio of TMB/P123 = 0.75) was slowly added. The mouth was sealed with plastic film. The mixed solution was stirred at 40°C for 24 h to produce milky gel liquid. It was then poured into a reactor on a Teflon substrate, and crystallized in an oven at 100°C for 48 h. Thereafter, it was taken out and cooled to room temperature. The product was filtered, washed with deionized water to remove residual liquid, then air-dried at room temperature. After drying, it was placed in a crucible, put in a muffle furnace, and calcined for 24 h to remove P123. At the end of the procedure, MCF white powder was obtained.

MCF modification
MCF powder (0.1 g) was poured into a 50 mL Beaker and subsequently added with 10 mL $EDTA$-Na_2 solution 0.1 mol/L. The mixture was stirred for 24 h at room temperature, thereafter, filtrated and washed. Modified MCF was obtained after it was air-dried at room temperature.

Batch adsorption of Hg^{2+} using modified MCF
The adsorbent, modified MCF, was added into 15 mL Hg^{2+} and stirred using a magnetic. The concentration of

Hg^{2+} ranged from 0.1 to 2 mg/mL. HNO_3 and NaOH solutions were used to obtain desirable pH levels (pH 1—5). The weight of the modified MCF varied between 0.05 and 0.3 g. The contact time and operating temperature were set within the range of 10—50 minutes and 25—45 ± 1°C, respectively. Afterward, the adsorbent was removed from the filtrate by centrifugation at 8000 r/min for 10 minutes. The final Hg^{2+} concentration in the filtrate was measured using A 722S spectrophotometer (Shanghai Prism Technology Co., Ltd., China) with a detailed procedure explained later.

The adsorption rate and adsorption capacity for Hg^{2+} were then calculated using Eq. 1 and 2, respectively [22, 29-31].

$$\text{Adsorption rate} = \frac{C_0 - C_e}{C_0} \times 100\% \qquad (1)$$

$$\text{Adsorption capacity } q_e = (C_0 - C_e) \times V/W \qquad (2)$$

Where C_0 (mg/mL) is the initial concentration of Hg^{2+}, Ce (mg/mL) is the concentration of Hg^{2+} at equilibrium, q_e (mg/g) is the adsorption capacity at equilibrium, V (mL) is the volume of solution, and W (g) is the adsorbent weight.

Spectrophotometric determination of mercury concentration

Preparation of chromogenic agent 5-Br-PADAP was conducted by dissolving 0.0175 g 5-Br-PADAP in 100 mL anhydrous ethanol. As for the sodium dodecyl sulfate, the solution was obtained by dissolving 1 g of sodium dodecyl sulfate into 100 mL of water. To measure 25 mL Hg^{2+} solution, 1.5 mL 0.0175% (w/v) 5-Br-PADAP anhydrous ethanol, 3.0 mL of pH 9.26 NH_4Cl-NH_3 buffer solution, and 3.0 mL of 0.1% (w/v) sodium dodecyl sulfate solution were added and left for 5 minutes. The concentration of mercury was then determined using A 722S spectrophotometer (Shanghai Prism Technology Co., Ltd., China) at wavelength 562 nm [32].

Adsorption kinetics

For the adsorption kinetics study, the Hg^{2+} solution with a variation of 0.4, 1.0, 1.6, 2.0, to 2.4 mg/mL was employed, the initial pH was adjusted to 3, modified MCF with a weight of 0.1 g was used, and the batch adsorption was carried out at room temperature.

Adsorption kinetics were studied using a quasi-first-order kinetic model [33-35] and a quasi-second-order kinetic model [34-36], expressed as follows

$$\log(q_e - q_t) = \lg q_e - k_1 t \qquad (3)$$

$$\frac{t}{q_t} = \frac{1}{k_2 q_e^2} + \frac{t}{q_e} \qquad (4)$$

Where k_1 (min⁻¹) represents the quasi-first-order kinetic rate constant, and the q_e and q_t (mg/g) are the adsorption capacity at equilibrium and the adsorption capacity (mg/g) at t (min); k_2 (g/mg.min) is a quasi-second-order kinetic rate constant.

Adsorption isotherm

The batch adsorption settings used in the adsorption isotherm study were similar to those of the previously explained kinetics isotherm study. The experimental data would be fitted to both Langmuir adsorption isotherm [37-40] and Freundlich adsorption isotherm models [34, 40, 41], mathematically expressed by Eq. (5) and (6), respectively.

$$\frac{C_e}{q_e} = \frac{1}{Q_0 b} + \left(\frac{1}{Q_0}\right) C_e \qquad (5)$$

$$\ln q_e = \ln K_F + \frac{1}{n} \ln C_e \qquad (6)$$

Where, Q_0 (mL/g) and b are the Langmuir constants related to the adsorption ability and adsorption rate. Meanwhile, K_F (mg/g) and n are Freundlich constants.

Desorption study

Firstly, a batch adsorption on 30 mL Hg^{2+} (1.0 mg/mL) was conducted using 0.1 g modified MCF at pH 3 and room temperature for 35 minutes. After separated from the filtrate, sediments were washed to obtain (modified MCF)-Hg sample. The mercury desorption was then conducted in 30 mL acid solution 0.1 mol/L (HNO_3 or HCl), where the mixture was stirred for 2—8 hours at room temperature. The adsorbent was removed from the solution by 10-minute centrifugation at 8000 r/min. The final Hg^{2+} concentration was calculated using the previously stated spectrophotometric procedure. The desorption rate was then calculated based on Eq. (7).

Desorption rate = desorption concentration / (7)
(initial   concentration − adsorption   equilibrium concentration) × 100%

Characterization

Siemens D5005 X-ray diffractometer, Germany, was used to determine the crystal phase structure and periodic

arrangement characteristics of the powder sample. Cu-Kα target, λ = 1.540560 Å, operating voltage (tube voltage) 50 kV, operating current (tube current) 150 mA, scan range 0.4°~ 10°and step size 0.02° were used. Philips XL30 field emission scanning electron microscope (SEM, Netherlands) was used to determine the SEM photographs to observe the particle size and morphology of the sample with an operating voltage 20 kV. The specific surface area, pore volume, and pore size distribution of the samples were investigated by nitrogen adsorption-desorption experiments. They were measured by an ASAP 2020V3.01H adsorption analyzer of American Micromerities at 77 K liquid nitrogen. The sample was activated by vacuum at 363 K for 12 h. The data was calculated by using the Bdb (Broekhoff and de Boer) method [42, 43]. The specific surface area was analyzed and calculated by BET (Brunner-Emmett-Teller) method [44] and the pore size distribution was analyzed and calculated by BJH (Barrett-Joyner-Halenda) method [45].

RESULTS AND DISCUSSION
Optimization of adsorption condition
Effect of pH

Solution pH could affect the surface state of the adsorbent and the ionization degree of an adsorbate [26, 27], which consequently affects the heavy metal uptake. The adsorption of Hg^{2+} onto modified MCF was found dependent on pH value, associated with the surface hydroxyl morphology and structure of the MCF material and the ionization degree of Hg^{2+}. In the case of $Hg(OH)_2$, its solubility is K_{sp} = 3.0 × 10^{-26}. Under the present experimental condition, pH level required to form $Hg(OH)_2$ is 2.54, where it is expected to completely precipitate with $[Hg^{2+}]$ = 1.0 × 10^{-6} mol/L at pH > 4.24. Hence, when pH level was increased greater than 4.24, the removal of Hg^{2+} was mainly derived from the precipitation of $Hg(OH)_2$. At pH < 2.54, the adsorption form of mercury on modified MCF mainly is Hg^{2+} and $Hg(OH)^+$ [46].

Experimental results (Fig.1-a) show that the rate of Hg^{2+} adsorption on the modified MCF was increased with the increase of pH in the range of 1.0 - 3.0. At a higher pH level, the solution would contain less competing H^+, which is favorable for the adsorptive removal of Hg^{2+}. However, a decrease on the adsorption rate began to observe after pH > 3.0. It is due to the emergence of $Hg(OH)_2$ precipitates, in which as a consequence, Hg^{2+} content would be relatively low. This condition further reduced the complexation rate between the EDTA in the MCF and Hg^{2+}. Since the Hg^{2+} adsorption rate is the highest at pH = 3.0, so all following experiments were carried out at pH 3.0.

Effect of contact time

The effect of contact time on Hg^{2+} adsorption is shown in Fig. 1-b. The adsorption efficiency and adsorption capacity of Hg^{2+} increased continuously during the first 35 minutes of batch adsorption. The adsorption rate and adsorption capacity were almost constant when the contact time was more than 35 min, which indicates that the adsorption process has reached an equilibrium. Rapid increases in the adsorption rate and adsorption capacity occur stem from the availability of unoccupied binding sites on the adsorbent surface. When most of the binding sites are occupied, as longer contact time is applied, the increased rate of Hg^{2+} uptake depletes gradually until the equilibrium is reached. In equilibrium, the desorption and adsorption rate of the adsorbate are equal giving a constant adsorption rate of Hg^{2+} [19, 20].

Effect of temperature

Fig. 1-c shows the relationship between temperature and Hg^{2+} adsorption rate. As the temperature increased, the adsorption rate of adsorbent to Hg^{2+} began to decrease slowly, which is an exothermic reaction. The effect of temperature on the adsorption was small, so the experiment was carried out at a room temperature $25 \pm 1°C$, and the room temperature was selected as the working temperature.

Effect of MCF dosage and Hg^{2+} concentration

Fig.1-d shows the effect of the adsorbent MCF amount. An increasing trend of adsorption rate and adsorption capacity of Hg^{2+} could be observed when the MCF dosage was increased from 0 to 0.1 g. It suggests the optimum MCF dosage was 0.1 g. Meanwhile, in the case of initial $[Hg^{2+}]$ variation, the adsorption rate and the adsorption capacity could be observed to increase when the initial concentration was increased from 0 to 0.1 mg/g (Fig. 1-e). With further increments of the mercury concentration, both the adsorption rate and the adsorption capacity decreased due to a decrease in the adsorption site of the adsorbent [34]. Under the above optimized experimental conditions, the adsorption capacity of mercury by the modified and
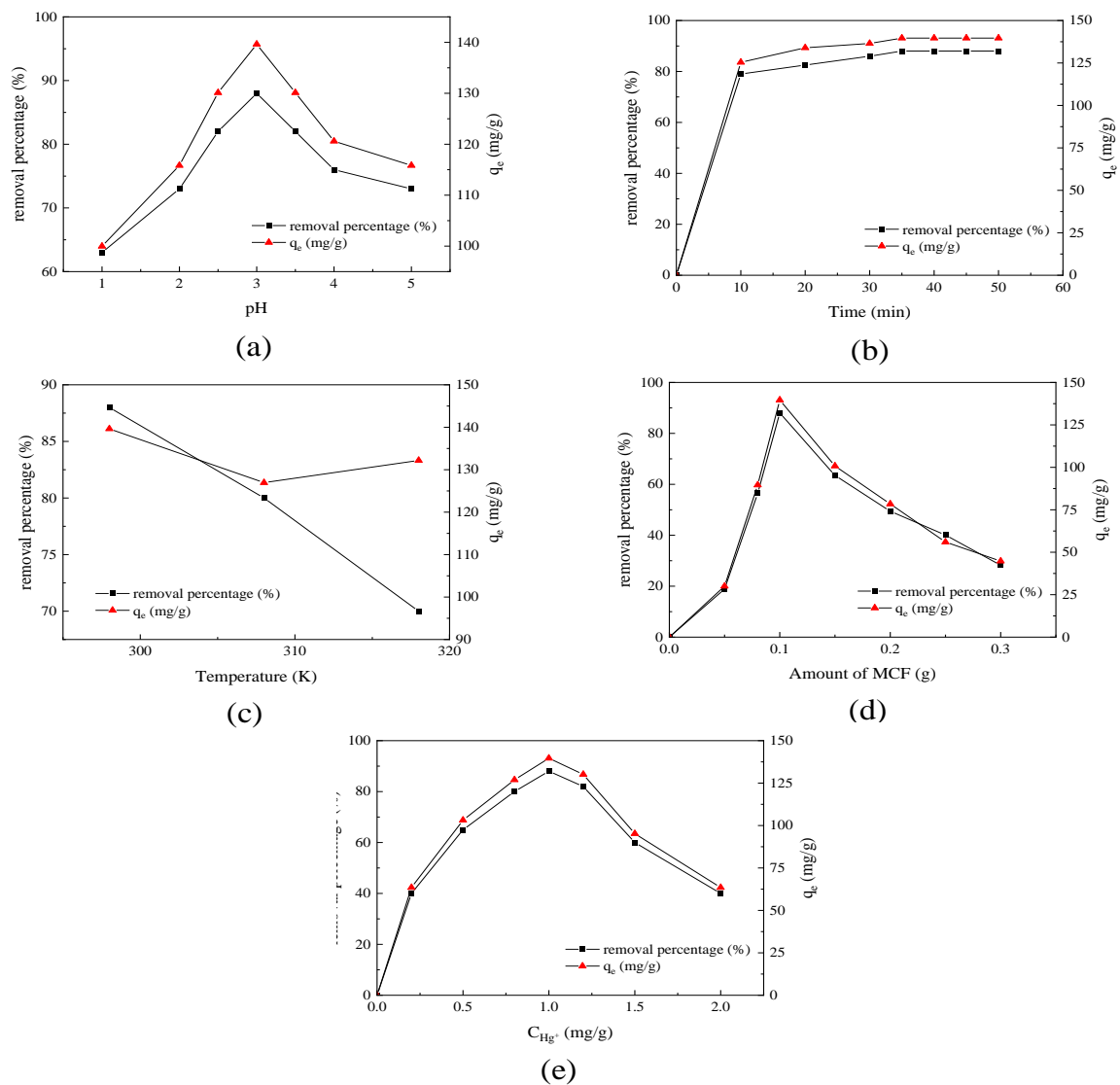
Fig. 1: Optimization of adsorption condition: (a) pH (adsorbent dosage 3.3 g/L, 25°C, contact time 35 min, [Hg²⁺] = 0.5 g/L),
(b) contact time (adsorbent dosage 3.3 g/L, 25°C, pH = 3.0, [Hg²⁺] = 0.5 g/L), (c) temperature (adsorbent dosage 3.3 g/L,
pH = 3.0, contact time 40 min, [Hg²⁺] = 0.5 g/L), (d) adsorbent dosage (pH = 3.0，contact time 40 min，[Hg²⁺] = 0.5 g/L) ,
(e) Hg²⁺ amount (pH = 3.0, contact time 40 min，adsorbent dosage 3.3 g/L).

unmodified materials were 139.64 mg/ g and 124.5 mg/g, respectively.

Table 1 gives a comparison of the adsorption capacity of this adsorbent for mercury (II) and other adsorbents [47-52]. From the Table, it can be seen that the adsorbent has a definite adsorption ability for mercury (II) compared with other adsorbents.

Adsorption kinetics

The experiment of adsorption kinetics was carried out by using different initial concentrations of Hg²⁺ at different contact times. The experimental results were linearly fitted with the quasi-first and quasi-second-order kinetic equations, respectively, respectively, and the results are shown in Fig. 2. The quasi-first-order and second-order kinetic data are shown in Table 2. As can be seen, the deviation of fitting data with a quasi-first-order kinetic equation is relatively large. However, the correlation coefficient (R_2^2) above 0.99 was obtained when the data fit with the quasi-second-order kinetic equation. The equilibrium adsorption capacity and the measured value of each concentration are not different, so the adsorption

Table 1: Comparison of various adsorbents: adsorption capacity for mercury(II) from aqueous medium.

Adsorbent	pH	Initial Hg^{2+} concentration (mg/L)	Adsorption capacity (mg/g)	Reference
SBA-15 functionalized by ethylenediaminopropyl	2.5	10	6.3	[47]
Amine-functionalized SBA-15 [(NH_2)-SBA-15]	3	10	7.59	[48]
Coal Fly Ash	3.5-4.5	5.5	5.85	[49]
-SH modified peat	7	600	175.439	[50]
Biochar of Coix Straw	6	100	235.3	[51]
Thiol-functionalized magnetic mesoporous silica material SH-$mSi@Fe_3O_4$	6.5	1	260	[52]
MCF-EDTA	3.0	1.0	139.64 mg / g	Present study

Table 2: Dynamic related parameters.

| Concentration (g/L)	Measured (mg/g)	Quasi-first adsorption rate equation			Quasi-second-order adsorption rate equation		
		k_1 (min^{-1})	q_e(mg/g)	R_1^2	k_2(g/mg min)	q_e(mg/g)	R_2^2
0.2	32.55	0.48798	537.03	0.9702	0.17315	32.79	1.0000
0.5	126.50	0.12107	295120	0.9294	0.02444	125.16	0.9997
0.8	132.14	0.08186	51286	0.6829	0.03776	129.87	0.9997
1.0	139.64	0.15916	1202264	0.6256	0.01967	138.50	0.9991
1.2	129.30	0.14816	123026	0.9415	0.03194	128.70	0.9999
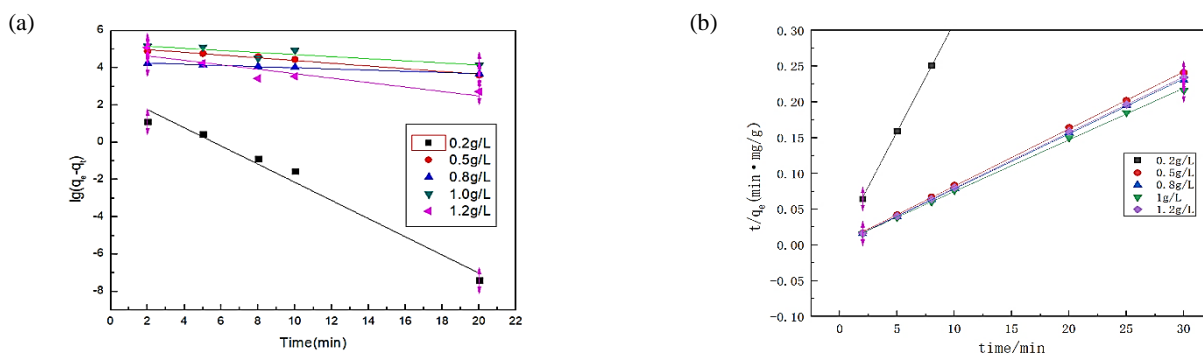
Fig. 2: Quasi-first-order (a) and quasi-second-order (b) dynamical equation images: (a) adsorbent dosage 3.3 g/L, 25 °C, pH = 3.0, (b) adsorbent dosage 3.3 g/L, 25 °C, pH = 3.0.

system much more accords with the quasi-second-order kinetic equation [40, 50-51].

Adsorption isotherms

Fig. 3 is the results of the linear fitting of the isotherm data of adsorbent for Hg^{2+} adsorption by Langmuir adsorption isotherm equation and Freundlich adsorption isotherm equation, respectively. The calculation results

of the corresponding related parameters are shown in Table 3. It can be seen that the correlation coefficient of the Langmuir adsorption isotherm is greater than 0.999 after fitting the experimental data and the adsorption capacity 139.64 mg/g that was obtained from the experiments is in agreement with the theoretical calculated value of 140.45 mg/g. Therefore, the Langmuir adsorption isotherm model describes

Table 3: Parameters associated with adsorption isotherm.

Temperature/K	Langmuir adsorption isotherm			Freundlich adsorption isotherm		
	Q_0 (mg/g)	b	R^2	K_F (L/g)	1/n	R^2
298.15	140.4494	49.7902	0.9996	140.054	0.0649	0.9878
308.15	138.6963	49.0476	0.9997	138.449	0.06641	0.9707
318.15	130.7190	61.1999	0.9998	130.342	0.05178	0.9845

(a)

(b)
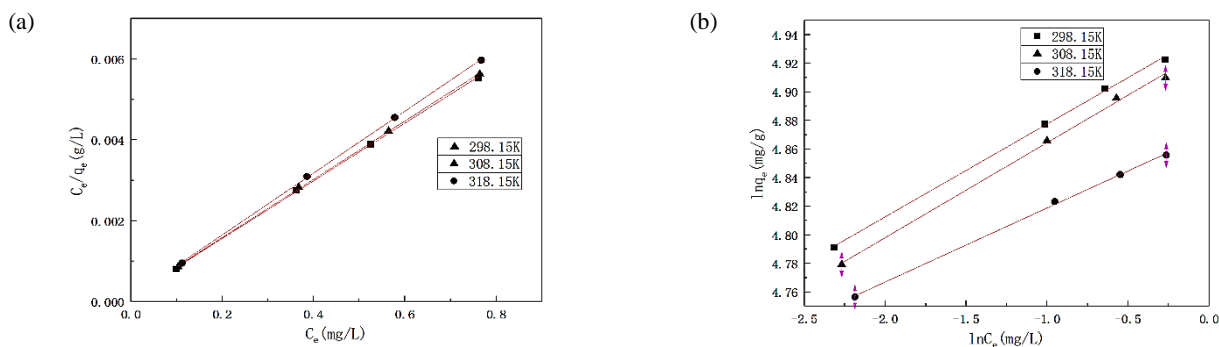
Fig. 3: Langmuir and Freundlich adsorption isotherm. (a) (adsorbent dosage 3.3 g/L, pH = 3.0),
(b) (adsorbent dosage 3.3 g/L, pH = 3.0).

the adsorption process, better than the Freundlich model, which represents monolayer adsorption [50-51].

Adsorption thermodynamics

The ΔG^0, ΔH^0, ΔS^0 during adsorption are derived from the following formula [30-31, 53-56]:

$$K_d = \frac{q_e}{C_e} \tag{8}$$

$$\Delta G^0 = -RT\ln K_d = \Delta H^0 - T\Delta S^0 \tag{9}$$

$$\ln K_d = -\Delta G^0 / (RT) = -\Delta H^0 / (RT) + \Delta S^0 / R \tag{10}$$

Where K_d is the equilibrium constant, q_e, C_e is the equilibrium adsorption capacity and the equilibrium adsorption concentration of adsorbate, ΔG^0 (kJ/mol) is the free energy variable value of the adsorption process, the gas constant R = 8.314 J/mol.K, T is the thermodynamic absolute temperature (K), ΔH^0 (kJ/mol) is the enthalpy change of adsorption process, ΔS^0 (J/mol·K) is the entropy change value of the adsorption process. The adsorption thermodynamic curve is obtained by plotting $\ln K_d$ versus 1/T.

Gibbs free energy ΔG^0, adsorption enthalpy ΔH^0, change adsorption entropy change ΔS^0 during the

adsorption process can be calculated according to the relevant formula, as shown in Table 4. As can be seen from Table 3, Gibbs free energy change in the process of Hg²⁺ adsorption by the EDTA-modified MCF, ΔG^0 is less than zero. The adsorption reaction was spontaneous. As can be seen from Table 4, the Gibbs free energy change of EDTA modified MCF adsorption Hg²⁺ process indicates that the adsorption reaction is spontaneous. It is generally considered that adsorption is physical adsorption when ΔG^0 is 0 - 20 kJ/mol [57]. Adsorption is physical and chemical adsorption when ΔG^0 is -20 to -80 kJ/mol. Adsorption is chemical adsorption when ΔG^0 is -80 to -400 kJ/mol. In this article ΔG^0 is in the range of 0 ~ -20 kJ/mol, therefore, the adsorption of Hg²⁺ by modified MCF should be physical adsorption. As can be seen from the calculation results, this adsorption $\Delta H^0 = $ -6.48 kJ/mol < 0, the reaction is exothermic. $\Delta S^0 = $ 37.43 J/(mol·K), shows that the adsorption process is the process of entropy increasing.

Desorption results

Fig. 4 shows the desorption results of Hg²⁺ using 0.10 mol/L HCl (Fig.4a) or HNO₃ (Fig.4b) solution. Through time, more Hg²⁺ can be desorbed and thus

Table 4: Thermodynamic parameters of adsorption.

Temperature (K)	ΔG^0 (kJ/mol)	ΔH^0 (kJ/mol)	ΔS^0 (J·mol^{-1}·K^{-1})
298.15	-17.61		
308.15	-18.05	-6.48	37.43
318.15	-18.36		

(a)

(b)
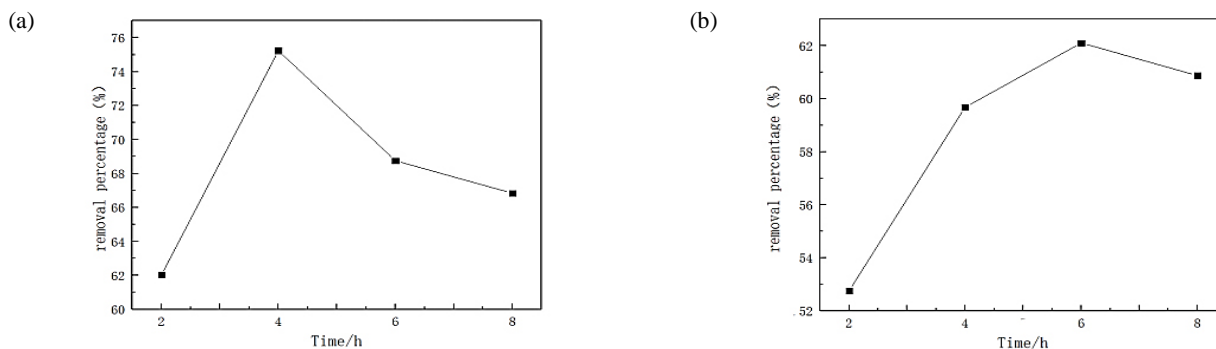
Fig.4: Desorption of composite materials: (a) desorption using 0.1 mol/L HCl, (b) desorption using 0.1 mol/L HNO₃.

the desorption rate gradually increased. For HCl or HNO₃ adsorbents, the desorption rate began to decrease when it reached 4 h or 6 h. Replacement of Hg^{2+} from the adsorbent surface by H^+ and the occurrence of desorption is a slow process. It takes some time to achieve desorption equilibrium. Therefore, before equilibrium is reached, the desorption rate is increased. However, after the equilibrium was reached, owing to the fact that the desorbed Hg^{2+} was again adsorbed on the adsorbent, this made the desorption rate increased a little decreased. At 4 or 6 h, the corresponding maximum desorption rate of HCl or HNO₃ was 75.23% and 62.10%, respectively. The previous result confirmed that HCl is better than HNO₃ and the optimum desorption time is 4 h. This result indicates that $HgCl_2$ stability is larger than the interaction between Hg^{2+} and modified MCF material.

Characterization of MCFs and their composite

The results of powder X-Ray Diffraction (XRD) analysis show the three characteristic diffraction peaks in MCF, EDTA-MCF, and EDTA-MCF-Hg(II) samples (Fig. 5), which can be assigned to diffraction peaks obtained from (100), (110) and (200) crystal plane diffraction. The data agreed with the peak position of MCF mesoporous materials reported by *Schmidt et al* [28]. Peak intensities of (b) and (c) are found to decrease, indicating that the degree of order of the pore channels in the MCF decreased after modification and adsorption processes. Scanning
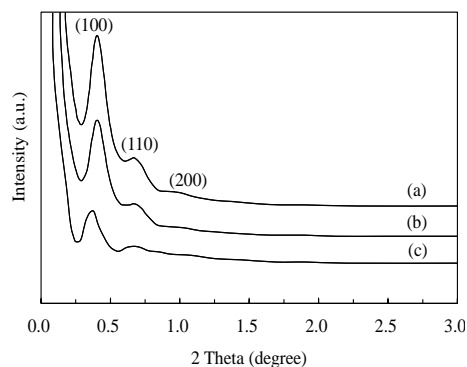
Fig. 5: Small angle X-Ray Diffraction (XRD) patterns of MCF (a), EDTA-MCF (b), EDTA- MCF-Hg (II) (c).

electron microscopy (SEM) results are shown in Fi.6. (a), (b) and (c) represent the SEM images of MCF, EDTA-MCF, and EDTA-MCF-Hg composites, respectively. As can be seen from the diagram, the shapes of the three samples are wheat spike-like structures, the mean diameter of the MCF is 2200 ± 10 nm, the mean diameter of the EDTA-MCF is 2250 ± 10 nm and the mean diameter of the EDTA-MCF-Hg(II) is 2270 ± 10 nm. It can be seen that the low-temperature N₂ adsorption-desorption isotherms and hysteresis loops of the three samples (MCF, EDTA-MCF, and EDTA-MCF-Hg) are basically close (Table 5). The data imply that after EDTA modification and adsorption of Hg^{2+}, the pore structure of MCF mesoporous

Table 5: Parameters of pore size structure of samples.

Sample	Spacing of crystal face d$_{100}$ (nm)	Cellular parameter, a$_0$ (nm)	Hole thickness (nm)	BET surface area (m^2/g)	Mesoporous volume (cm^3/g)	Average hole diameter, D$_p$ (nm)
MCF	19.19	22.16	11.75	585	1.36	10.41
MCF-EDTA	18.44	21.30	13.61	427	0.81	7.69
MCF-EDTA-Hg(II)	17.65	20.45	12.85	400	0.60	7.60

Note : cell parameter $a_0 = \frac{2}{\sqrt{3}} d_{100}$, *average pore diameter* $D_p = 4V_{mes} / S_{BET}$, V_{mes} *mesoporous volume,* S_{BET} *BET surface area; hole thickness* $= a_0 - D_p$.
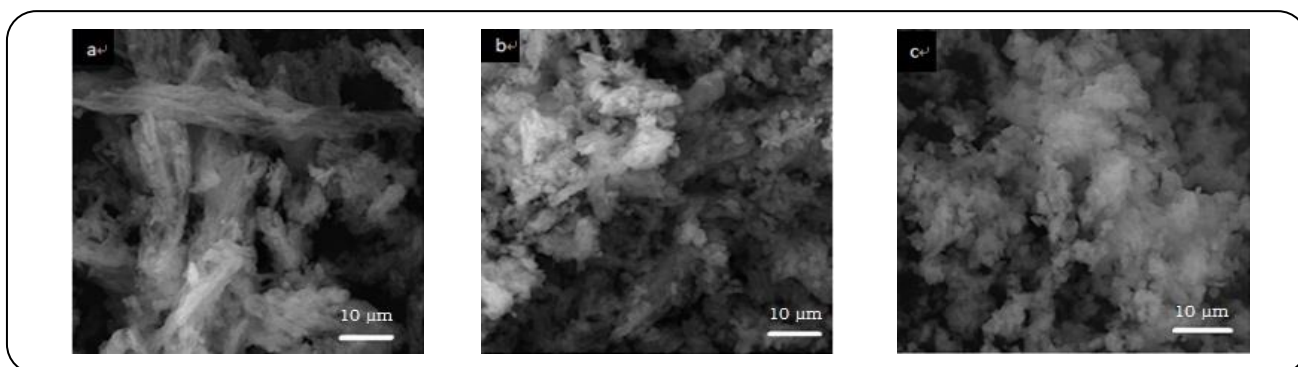

Fig. 6. SEM images of MCF(a), EDTA-MCF(b), EDTA-MCF-Hg(II)(c).

materials remained intact. After the MCF was modified by EDTA and adsorbed Hg^{2+}, it is obvious that the isotherm and the relative partial pressure range would gradually decrease. Moreover, the gradual reduction in BET-specific surface area suggests that EDTA and Hg^{2+} have occupied the MCF channels, instead of attached on its outer surface.

CONCLUSIONS

EDTA modification on MCF has been proven capable of improving its performance in the removal of aqueous Hg^{2+} through the batch adsorption process. Langmuir adsorption isotherm is better to represent the adsorption process suggesting that the adsorption is monolayer. The Gibbs free energy change of adsorption Hg^{2+} onto EDTA-modified MCF process indicates that the adsorption reaction occurred spontaneously. The adsorption reaction was exothermic and the adsorption process was the process of increasing entropy. The adsorption process conforms to the quasi-second-order kinetic equation.

REFERENCES

[1] Cheng X., Heavy Metal Pollution Needs Urgent Attention in Taihu Basin, *Water Resour. Protect.*, **4**:39-41(2002).

[2] Zhou Q. Y., Li G. C., Tang Z. C., Research on the Status and Treatment of Heavy Metal Pollution in China, *Light Ind. Technol.*, **4**:98-99 (2013).

[3] Ding X.Y., Tang S.X., Ecological Purification Effect of Plant and Basalt on Heavy Metals in Water, *Anhui Agricul. Sci.*, **47**:60-63 (2019).

[4] Boening D.W., Ecological Effects, Transport, and Fate of Mercury: A General Review, *Chemosphere*, **40(12)**: 1335-1351(2000).

[5] Guo Y.N., Fang Z.K., Hu J. H., Progress in the Treatment of Wastewater Containing Heavy Metals by Chemical Precipitation, *Ind. Water Treat.*, **31**:9-13 (2011).

[6] Azzam A.M., El-Wakeel S.T., Mostafa B.B., El-Shahat M.F., Removal of Pb, Cd, Cu, and Ni from Aqueous Solution Using Nano-Scale Zero Valent Iron Particles, *J. Env. Chem. Eng.*, **4(2)**:2196-2206 (2016).

[7] Wang S.G., Wang K.K., Dai C., Shi H.Z., Li J.L., Adsorption of Pb^{2+} on Amino-functionalized Core–shell Magnetic Mesoporous SBA-15 Silica Composite, *Chem. Eng. J.*, **262**:897-903 (2015).

[8] Guo R.Q., Chai S.Q., Mao J.T., Synthesis of a Modified Chelating Resin and Its Adsorption and Desorption of Hg^{2+} of Water Body, *Environ. Sci. Technol.*, **31**:14-19 (2013).

[9] Wu J., Li Q. B., Deng X., Lu Y. H., Research Advance of Heavy Metals by Biological Adsorption, *Ion Exch. Adsor.*, **14**: 180-187 (1998).

[10] Guo Y.Q., Song L., Progress of Heavy Metal Wastewater Pollution and Its Control Technology, *Guangzhou Chem. Indus.*, **38**:18-20 (2010).

[11] Fu F., Wang Q., Removal of Heavy Metal Ions from Wastewaters: A Review, *J. Environ. Manage.*, **92**: 407-418 (2011).

[12] Gupta S., Sharma S. K., Kumar A., Biosorption of Ni(II) Ions from Aqueous Solution Using Modified Aloe Barbadensis Miller Leaf Powde, Water Sci. Eng.**, 12**:27 (2019).

[13] Zenasni M.A., Benfarhi S., Merlin A., Molina S., George B., Meroufel1 B. Adsorption of Nickel in Aqueous Solution onto Natural Maghnite, *Mater. Sci. Appl.*, **4**:153-161 (2013).

[14] Ahmed, A.M.M., Ali, A.E., Ghazy, A.H., Adsorption Separation of Nickel from Wastewaterby Using Olive Stones, *Adv. J. Chem.-Section A*, **2**:79-93 (2019).

[15] Ghorbani M., Nowee S.M., Ramezanian N, Raji F., A New Nanostructured Material Amino Functionalized Mesoporous Silica Synthesized Via Co-condensation Method for Pb(II) and Ni(II) Ion Sorption from Aqueous Solution, *Hydrometallurgy*, **161**:117-126 (2016).

[16] Xue X.M., Li F.T., Removal of Cu(II) From Aqueous Solution by Adsorption onto Functionalized SBA-16, *Micropor. Mesopor. Mater.*, **116(1-3)**:116-122 (2008).

[17] Dana E, Sayari A. Adsorption of Copper on Amine-functionalized SBA-15 Prepared by Co-condensation: Equilibrium Properties, *Chem. Eng. J.*, **166**:445-453 (2011).

[18] Li Y., Bai P., Yan Y., Yan W., Shi W., Xu R., Removal of Zn^{2+}, Pb^{2+}, Cd^{2+}, and Cu^{2+} from Aqueous Solution by Synthetic Clinoptilolite, *Micropor. Mesopor. Mater.*, **273**:203-211 (2019).

[19] Shahbazi A., Younesi H., Badiei A., Batch and Fixed-Bed Column Adsorption of Cu(II), Pb(II) and Cd(II) from Aqueous Solution onto Functionalised SBA-15 Mesoporous Silica, *Can. J. Chem. Eng.*, **99:**1-12 (2012).

[20] Wang S.G., Wang K.K., Dai C., Shi H.Z., Li J.L., Adsorption of Pb^{2+} on Amino-functionalized Core–shell Magnetic Mesoporous SBA-15 Silica Composite, *Chem. Eng. J.*, **262**:897-903 (2015).

[21] Liu Y., Pan J. M., Chen J., Xie J. M., Li C.X., Yan Y.S., Progress of Modified Silica-Based Micro/Nano Materials and Their Application in Separation Chemistry, *Metall. Anal.*, **30**:37-46 (2012).

[22] Rahmi L., Iqhrammullah M., Audina U., Husin H., Fathana H., Adsorptive Removal of Cd(II) Using Oil Palm Empty Fruit Bunch-Based Charcoal/Chitosan-EDTA Film Composite, *Sustain. Chem. Pharm.*, **21**:100449 (2021).

[23] Zhao P.Y., Zhang G.J., Xu Y., Lv Y.K., Yang Z.X., Cheng H.Z., Development of Amine-functionalized Silica Foams with Hierarchical Pore Structure for CO_2 Capture, *Energ. Fuel.*, **33**:3357-3369 (2019).

[24] Wijesiri R.P., Knowles G.P., Yeasmin H., Hoadley A.F.A., Chaffee A.L., CO_2 Capture from Air Using Pelletized Polyethylenimine Impregnated MCF Silica, *Ind. Eng. Chem. Res.*, **58**:3293-3303 (2019).

[25] Daoura O., Daher S., Kaydouh M.N., Hassan N.E., Massiani P., Launay F., Boutros M., Influence of the Swelling Agents of Siliceous Mesocellular Foams on the Performances of Ni-based Methane Dry Reforming Catalysts, *Int. J. Hydrog. Energy*, **43(36)**:17205-17215 (2018).

[26] He R., Wang Z.H., Tan L., Zhong Y., Li W.M., Xing D., Wei C.H., Tang Y.W., Design and Fabrication of Highly Ordered Ion Imprinted SBA-15 and MCM-41 Mesoporous Organosilicas for Efficient Removal of Ni^{2+} from Different Properties of Wastewaters, Micropor. Mesopor. Mater., **257**:212-221 (2018).

[27] Wang S.G., Wang K.K., Dai C., Shi H.Z., Li J.L., Adsorption of Pb^{2+} on Amino-functionalized Core–shell Magnetic Mesoporous SBA-15 Silica Composite, *Chem. Eng. J.*, **262**:897-903 (2015).

[28] Schmidt W.P., Lukens W.W., Zhao D.Y., Yang P., Chmelka B.F., Stucky G.D., Mesocellular Siliceous Foams with Uniformly Sized Cells and Windows, *J. Am. Chem. Soc.*, **121**:254-255 (1999).

[29] Myneni V.R., Punugoti T., Kala N.S., Kanidarapu N.R., Vangalapati M., Modelling and Optimization of Methylene Blue Adsorption onto Magnesium Oxide Nanoparticles Loaded onto Activated Carbon (MgONP-AC): Response Surface Methodology and Artificial Neural Networks, *Mater. Today: Proceed.*, **18**:4932-4941 (2019).

[30] Jawad A.H., Norrahma S.S.A., Hameed B.H., Ismail K., Chitosan-Glyoxal Film as a Superior Adsorbent for Two Structurally Different Reactive and Acid Dyes: Adsorption and Mechanism Study, *Int. J. Biol. Macromal.*, **135**:569-581 (2019).

[31] Jawad A.H., Mohammed I.A., Abdulhameed A.S., Tuning of Fly Ash Loading into Chitosan-Ethylene Glycol Diglycidyl Ether Composite for Enhanced Removal of Reactive Red 120 Dye: Optimization Using the Box-Behnken Design, *J. Polym. Environ.*, **28**:2720-2733 (2020).

[32] Liu J.H., Huang C.X., Huang Y., Spectrophotometric Study on the Reaction of 5-Br-PADAP with Mercury (II) in the Presence of Surfactant, *Phys. Test. Chem. Anal.*, **35B(5)**:218-219 (1999).

[33] Lagergren S., Zur Theorie Der Sogenannten Adsorption Geloester Stoffe (About the Theory of So-called Adsorption of Soluble Substances), *Kungliga Svenska Vetenskapsakademiens Handlingar Band*, **24**:1-39 (1898).

[34] Crini G., Peindy H.N., Gimbert F., Robert C., Removal of C. I. Basic Green 4 (Malachite Green) from Aqueous Solution by Adsorption using Cyclodextrin-based Adsorbent: Kinetic and Equilibrium Studies, *Sep. Purif. Technol.* **53**: 97-110 (2007).

[35] Naushad M., Surfactant Assisted Nano-Composite Cation Exchanger: Development, Characterization and Applications for the Removal of Toxic Pb²⁺ from Aqueous Medium, *Chem. Eng. J.*, **235**:100-108 (2014).

[36] Ho Y.S., McKay G., Pseudo-second Order Model for Sorption Processes, Process Biochem., **34(5)**:451-465 (1999).

[37] Langmuir I., The Constitution and Fundamental Properties of Solids and Liquids, *J. Am. Chem. Soc.*, **38(11)**:2221-2295 (1916).

[38] Langmuir I., The Adsorption of Gases on Plane Surfaces of Glass, Mica and Platinum, *J. Am. Chem. Soc.*, **40(9)**:1361-1403 (1918).

[39] Alqadami A.A., Naushad M., Alothman Z.A., Ghfar A.A., Novel Metal-organic Framework (MOF) Based Composite Material for the Sequestration of U(VI) and Th(IV) Metal Ions from Aqueous Environment, *ACS Appl. Mater. Interf.*, **9(41)**: 36026-36037 (2017).

[40] Rahmi R., Lubis S., Az-Zahra N., Puspita K., Iqhrammullah M., Synergetic Photocatalytic and Adsorptive Removals of Metanil Yellow Using TiO₂/Grass-Derived Cellulose/Chitosan (TiO₂/GC/CH) Film Composite, *IJE Transactions B: Appl.* , *Int. J. Eng.*, **34(8)**:1827-1836 (2021).

[41] Freundlich H.M.F., Uber Die Adsorption in Losungen, *Z Phys. Chem.*, **57**:385-471 (1906).

[42] Broekhoff J.C.P., De Boer J.H., Studies on Pore Systems in Catalysts: XI. Pore Distribution Calculations from the Adsorption Branch of a Nitrogen Adsorption Isotherm in The Case of "Ink-Bottle" Type Pores, *J. Catal.*, **10**:153-165 (1968).

[43] Broekhoff J.C.P., De Boer J.H., Studies on Pore Systems in Catalysts: XII. Pore Distributions from The Desorption Branch of a Nitrogen Sorption Isotherm in the Case of Cylindrical Pores: A. An Analysis of the Capillary Evaporation Process, *J. Catal*., **10(4)**: 368-376 (1968).

[44] Brunauer S., Emmett P.H., Teller E., Adsorption of Gases in Multimolecular Layers, *J. Am. Chem. Soc.*, **60**:309-319 (1938).

[45] Barrett E.P., Joyner L.G., Halenda P.P., The Determination of Pore Volume and Area Distributions in Porous Substances. I. Computation from Nitrogen Isotherms, *J. Am. Chem. Soc.*, **73**:373-380 (1951).

[46] Wuhan University, "Analytical Chemistry (Second Edition)", Higher Education Press, Beijing, P.R. China p.592 (1982).

[47] Dindar M.H., Yaftian M.R., Hajihasani M., Rostamnia S., Refinement of Contaminated Water by Cr(VI), As(V) and Hg(II) Using N-Donor Ligands Arranged on SBA-15 Platform; Bath and Fixed-Bed Column Methods, *J. Taiwan. Inst. Chem.*, **67**:325-337 (2016).

[48] Dindar M.H., Yaftian M.R., Rostamnia S., Potential of Functionalized SBA-15 Mesoporous Materials for Decontamination of Water Solutions from Cr(VI), As(V) and Hg(II) Ions, *J. Environ. Chem. Eng.*, **3(2)**:986-995 (2015).

[49] Sen A.K., De A.K., Adsorption of Mercury(II) by Coal Fly Ash, *Water Res.*, **21(8)**: 885-888.

[50] Yao C., He T.R., Ran S., Wang Z.B., Wang H., Adsorption and Desorption of Hg^{2+} in Water by Thiol Group Modified Peat, *Indus. Water Treat.*, **40 (10)**:67-71 (2020).

[51] Zhang B.B., Yang Z., Xue B., Ding X.Y., Lou J.F., Wang S., Chen W.J., Xu G.M., Adsorption of Aquatic Hg^{2+} by Biochar Obtained from Coix Straw, *Ecol. Environ. Sci.*, **30 (5)**:1051-1059 (2021).

[52] Li G.L., Zhao Z.S., Liu J.Y., Jiang G.B., Effective Heavy Metal Removal from Aqueous Systems by Thiol Functionalized Magnetic Mesoporous Silica, *J. Hazard. Mater.*, **192(1)**: 277-283 (2011).

[53] Chowdhury S., Mishra R., Saha P., Kushwaha P., Adsorption Thermodynamics, Kinetics and Isosteric Heat of Adsorption of Malachite Green onto Chemically Modified Rice Husk, *Desalination*, **265(1-3)**: 159-168 (2011).

[54] Zhou Y.M., Zhang M., Hu X.Y., Wang X.H., Niu J.Y., Ma T.S., Adsorption of Cationic Dyes on a Cellulose-Based Multicarboxyl Adsorbent, *J. Chem. Eng. Data***, 58**: 413-421 (2013).

[55] Naushad M., Ahamad T., Sharma G., Albadarin A.B., Alam M.M., Alothman Z.A., Alshehri S. M., Ghfar A.A., Synthesis and Characterization of a New Starch/SnO_2 Nanocomposite for Efficient Adsorption of Toxic Hg^{2+} Metal Ion, *Chem. Eng. J.*, **300**:306-316 (2016).

[56] Jawad A.H., Ismail K., Ishak M.A.M., Wilson L.D., Conversion of Malaysian Low-Rank Coal to Mesoporous Activated Carbon: Structure Characterization and Adsorption Properties, *Chin. J. Chem. Eng.*, **27(7)**: 1716-1727 (2019).

[57] Gerçel O., Ozcan A., Ozcan A.S., Gercel H.F., Preparation of Activated Carbon from a Renewable Bio-plant of Euphorbia Rigida, by H_2SO_4 Activation and its Adsorption Behavior in Aqueous Solutions, *Appl. Surf. Sci.*, **253**:4843-4852 (2007).